Integrated autocorrelator based on superconducting nanowires

Döndü Sahin,[1,*] Alessandro Gaggero,[2] Thang Ba Hoang,[1] Giulia Frucci,[1] Francesco Mattioli,[2] Roberto Leoni,[2] Johannes Beetz,[3] Matthias Lermer,[3] Martin Kamp,[3] Sven Höfling,[3] and Andrea Fiore[1]

[1]*COBRA Research Institute, Eindhoven University of Technology, PO Box 513, 5600 MB Eindhoven, The Netherlands*

[2]*Istituto di Fotonica e Nanotecnologie, CNR, via Cineto Romano 42, 00156 Roma, Italy*

[3]*Technische Physik, Julius-Maximilians-Universität Würzburg, Physikalisches Institut and Wilhelm Conrad Röntgen-Center for Complex Material Systems, Am Hubland, 97074 Würzburg, Germany*

[*]*d.sahin@tue.nl*

Abstract: We demonstrate an integrated autocorrelator based on two superconducting single-photon detectors patterned on top of a GaAs ridge waveguide. This device enables the on-chip measurement of the second-order intensity correlation function $g^{(2)}(\tau)$. A polarization-independent device quantum efficiency in the 1% range is reported, with a timing jitter of 88 ps at 1300 nm. $g^{(2)}(\tau)$ measurements of continuous-wave and pulsed laser excitations are demonstrated with no measurable crosstalk within our measurement accuracy.

OCIS codes: (130.3120) Integrated optics devices; (270.5570) Quantum detectors.

References and links

1. D. Englund, A. Faraon, B. Zhang, Y. Yamamoto, and J. Vucković, "Generation and transfer of single photons on a photonic crystal chip," Opt. Express **15**(9), 5550–5558 (2007).
2. A. Schwagmann, S. Kalliakos, I. Farrer, J. P. Griffiths, G. A. C. Jones, D. A. Ritchie, and A. J. Shields, "On-chip photon emission from an integrated semiconductor quantum dot into a photonic crystal waveguide," Appl. Phys. Lett. **99**(26), 261108 (2011).
3. T. B. Hoang, J. Beetz, M. Lermer, L. Midolo, M. Kamp, S. Höfling, and A. Fiore, "Widely tunable, efficient on-chip single photon sources at telecommunication wavelengths," Opt. Express **20**(19), 21758–21765 (2012).
4. A. Laucht, S. Pütz, T. Günthner, N. Hauke, R. Saive, S. Frédérick, M. Bichler, M.-C. Amann, A. W. Holleitner, M. Kaniber, and J. J. Finley, "A waveguide-coupled on-chip single-photon source," Phys. Rev. X **2**(1), 011014 (2012).
5. A. Politi, M. J. Cryan, J. G. Rarity, S. Yu, and J. L. O'Brien, "Silica-on-silicon waveguide quantum circuits," Science **320**(5876), 646–649 (2008).
6. J. P. Sprengers, A. Gaggero, D. Sahin, S. Jahanmirinejad, G. Frucci, F. Mattioli, R. Leoni, J. Beetz, M. Lermer, M. Kamp, S. Höfling, R. Sanjines, and A. Fiore, "Waveguide superconducting single-photon detectors for integrated quantum photonic circuits," Appl. Phys. Lett. **99**(18), 181110 (2011).
7. T. Gerrits, N. Thomas-Peter, J. C. Gates, A. E. Lita, B. J. Metcalf, B. Calkins, N. A. Tomlin, A. E. Fox, A. L. Linares, J. B. Spring, N. K. Langford, R. P. Mirin, P. G. R. Smith, I. A. Walmsley, and S. W. Nam, "On-chip, photon-number-resolving, telecommunication-band detectors for scalable photonic information processing," Phys. Rev. A **84**(6), 060301 (2011).
8. W. H. P. Pernice, C. Schuck, O. Minaeva, M. Li, G. N. Goltsman, A. V. Sergienko, and H. X. Tang, "High-speed and high-efficiency travelling wave single-photon detectors embedded in nanophotonic circuits," Nat Commun **3**, 1325 (2012).
9. G. Reithmaier, S. Lichmannecker, T. Reichert, P. Hasch, M. Bichler, R. Gross, and J. J. Finley, "On-chip time resolved detection of quantum dot emission using integrated superconducting single photon detectors," arxiv:1302.3807 (2013).
10. C. Schuck, W. H. P. Pernice, and H. X. Tang, "NbTiN superconducting nanowire detectors for visible and telecom wavelengths single photon counting on Si_3N_4 photonic circuits," Appl. Phys. Lett. **102**(5), 051101 (2013).
11. A. A. Guzik and P. Walther, "Photonic quantum simulators," Nat. Phys. **8**(4), 285–291 (2012).
12. A. J. Shields, "Semiconductor quantum light sources," Nat. Photonics **1**(4), 215–223 (2007).
13. R. Hanbury Brown and R. Q. Twiss, "A test of a new type of stellar interferometer on Sirius," Nature **178**(4541), 1046–1048 (1956).

#185466 - $15.00 USD Received 15 Feb 2013; revised 19 Apr 2013; accepted 22 Apr 2013; published 30 Apr 2013

14. E. A. Dauler, B. S. Robinson, A. J. Kerman, J. K. W. Yang, K. M. Rosfjord, V. Anant, B. Voronov, G. Gol'tsman, and K. K. Berggren, "Multi-element superconducting nanowire single-photon detector," IEEE Trans.on Appl. Supercond. **17**(2), 279–284 (2007).
15. A. Divochiy, F. Marsili, D. Bitauld, A. Gaggero, R. Leoni, F. Mattioli, A. Korneev, V. Seleznev, N. Kaurova, O. Minaeva, G. Gol'tsman, K. G. Lagoudakis, M. Benkhaoul, F. Lévy, and A. Fiore, "Superconducting nanowire photon-number-resolving detector at telecom wavelength," Nat. Photonics **2**(5), 302–306 (2008).
16. S. Jahanmirinejad, G. Frucci, F. Mattioli, D. Sahin, A. Gaggero, R. Leoni, and A. Fiore, "Photon-number resolving detector based on a series array of superconducting nanowires," Appl. Phys. Lett. **101**(7), 072602 (2012).
17. G. N. Gol'tsman, O. Okunev, G. Chulkova, A. Lipatov, A. Semenov, K. Smirnov, B. Voronov, A. Dzardanov, C. Williams, and R. Sobolewski, "Picosecond superconducting single-photon optical detector," Appl. Phys. Lett. **79**(6), 705–707 (2001).
18. V. Anant, A. J. Kerman, E. A. Dauler, J. K. W. Yang, K. M. Rosfjord, and K. K. Berggren, "Optical properties of superconducting nanowire single-photon detectors," Opt. Express **16**(14), 10750–10761 (2008).
19. A. Gaggero, S. Jahanmiri Nejad, F. Marsili, F. Mattioli, R. Leoni, D. Bitauld, D. Sahin, G. J. Hamhuis, R. Notzel, R. Sanjines, and A. Fiore, "Nanowire superconducting single-photon detectors on GaAs for integrated quantum photonic applications," Appl. Phys. Lett. **97**(15), 151108 (2010).
20. F. Marsili, "Single-photon and photon-number-resolving detectors based on superconducting nanowires," PhD dissertation, École Polytechnique Fédérale De Lausanne, Chap. 2.
21. D. Sahin, A. Gaggero, G. Frucci, S. Jahanmirinejad, J. P. Sprengers, F. Mattioli, R. Leoni, J. Beetz, M. Lermer, M. Kamp, S. Höfling, and A. Fiore, "Waveguide superconducting single-photon autocorrelators for quantum photonic applications," Proc. SPIE **8635**, 86351B, 86351B-6 (2013).
22. F. Marsili, D. Bitauld, A. Gaggero, S. Jahanmirinejad, R. Leoni, F. Mattioli, and A. Fiore, "Physics and application of photon number resolving detectors based on superconducting parallel nanowires," New J. Phys. **11**(4), 045022 (2009).
23. F. Marsili, F. Najafi, E. Dauler, F. Bellei, X. Hu, M. Csete, R. J. Molnar, and K. K. Berggren, "Single-Photon Detectors Based on Ultranarrow Superconducting Nanowires," Nano Lett. **11**(5), 2048–2053 (2011).
24. T. Yamashita, S. Miki, H. Terai, K. Makise, and Z. Wang, "Crosstalk-free operation of multielement superconducting nanowire single-photon detector array integrated with single-flux-quantum circuit in a 0.1 W Gifford-McMahon cryocooler," Opt. Lett. **37**(14), 2982–2984 (2012).
25. K. S. Ilin, M. Lindgren, M. Currie, A. D. Semenov, G. N. Gol'tsman, R. Sobolewski, S. I. Cherednichenko, and E. M. Gershenzon, "Picosecond hot-electron energy relaxation in NbN superconducting photodetectors," Appl. Phys. Lett. **76**(19), 2752–2754 (2000).
26. Z. Zhou, G. Frucci, F. Mattioli, A. Gaggero, R. Leoni, S. Jahanmirinejad, T. B. Hoang, and A. Fiore, "Ultrasensitive N-photon interferometric autocorrelator," Phys. Rev. Lett. **110**(13), 133605 (2013).
27. A. Korneev, Y. Vachtomin, O. Minaeva, A. Divochiy, K. Smirnov, O. Okunev, G. Gol'tsman, C. Zinoni, N. Chauvin, L. Balet, F. Marsili, D. Bitauld, B. Alloing, L. Li, A. Fiore, L. Lunghi, A. Gerardino, M. Halder, C. Jorel, and H. Zbinden, "Single-photon detection system for quantum optics applications," IEEE J. Sel. Top. Quantum Electron. **13**(4), 944–951 (2007).

1. Introduction

For advancing quantum photonics, the integration of optical components, such as single photon sources [1–4], passive circuit elements [5] and single photon detectors [6–10], within a quantum photonic integrated circuit (QPIC) is required in order to scale the system up to few tens of photons, which would be for example required to perform quantum simulations [11]. The measurement of the second-order correlation function $g^{(2)}(\tau)$ and of the photon number is a key functionality for such a QPIC, allowing for example the characterization of single- and entangled-photon states [12]. The second-order autocorrelation function is usually measured in free space or fiber-optics with a Hanbury-Brown and Twiss interferometer [13], using a 50:50 beamsplitter and two distinct detectors on the two output arms. That allows overcoming the dead-time limitation of single-photon detectors. An alternative but equivalent approach is to illuminate two or more detectors with the optical beam under test, as demonstrated in free-space optics using superconducting nanowire single photon detectors [14].

In this work, we apply a similar concept in an *integrated* platform and demonstrate an intensity autocorrelator based on two superconducting nanowires sensing the evanescent field of the same waveguide mode. This enables the measurement of the $g^{(2)}(\tau)$ with a very compact integrated device and represents the first step towards integrated photon-number-resolving detectors [15,16]. We report the polarization-independent response of the integrated nanowires and a detailed study of their mutual coupling, showing no measurable static and dynamic crosstalk.

#185466 - $15.00 USD Received 15 Feb 2013; revised 19 Apr 2013; accepted 22 Apr 2013; published 30 Apr 2013

2. Concept, design and fabrication

Figure 1(a) (sketch) shows the schematics of the integrated autocorrelators on a GaAs (0.35 μm)/$Al_{0.75}Ga_{0.25}As$ (1.5 μm) waveguide heterostructure. There are two pairs of equidistant NbN nanowires on top of the waveguide, each with a width of 100 nm, a length of 50 μm and a spacing of 150 nm. Each pair of nanowires is separately connected to a bias and amplification circuit. The two pairs therefore constitute two independent superconducting single-photon detectors. The detectors exploit the hotspot mechanism for photon detection [17]. A single absorbed infrared photon breaks a Cooper pair which, through a subsequent relaxation process, creates a non-equilibrium population of quasi-particles. The resulting perturbation can produce a resistive cross-section in the wire, which diverts the bias current to a parallel load resistor, producing a voltage pulse.

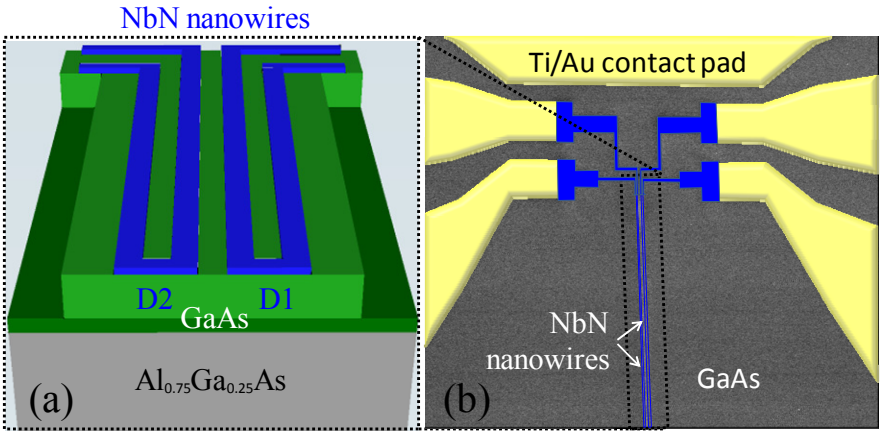

Fig. 1: (a) Schematics of the integrated autocorrelators with two, electrically-separated single-photon detectors on top of GaAs ridge waveguide and (b) False-color scanning electron microscope image of two-element waveguide detectors.

The symmetric design assures the equal coupling of the waveguide mode with the two pairs of nanowires on the waveguide. The GaAs core layer is etched down by 300 nm to create a 1.85 μm-wide ridge waveguide that confines the quasi-transverse electric (TE) and transverse magnetic (TM) modes. In our simulations, we consider a 100 nm-thick SiO_x layer that is left as a residue of the hydrogen silsesquioxane (HSQ) on top of the NbN nanowires after the patterning of the nanowires. The modal absorption coefficients calculated with a finite-element solver (Comsol Multiphysics) are $\alpha_{TE} = 542\ cm^{-1}$ and $\alpha_{TM} = 758\ cm^{-1}$ for the lowest-order quasi-TE and quasi-TM modes (assuming a 5.9 nm-thick NbN layer and a refractive index $n_{NbN} = 5.23 - 5.82i$ [18]), respectively. That allows 93% TE and 98% TM mode absorptance along a 50 μm-long waveguide.

A GaAs /$Al_{0.75}Ga_{0.25}As$ heterostructure is grown by molecular beam epitaxy on top of an undoped GaAs (001) substrate. On the GaAs epi-layer, a 5.9 nm-thick NbN superconducting film is grown by a DC magnetron reactive sputtering technique in an Ar + N_2 ambient at a nominal temperature of 415 °C with a critical temperature of $T_c = 10.1$ K and a transition width of $\Delta T_c = 0.5$ K [19]. The T_c and ΔT_c are determined using the average and the difference of the temperatures corresponding to 90% and 10% of the average normal resistance derived following the procedure in Ref [20]. The autocorrelators are fabricated using four steps of direct-writing electron beam lithography (EBL). In the first step Ti(10nm)/Au(60nm) contact pads (patterned as a 50 Ω coplanar transmission line) and alignment markers are defined on positive tone PMMA electronic resist by lift-off. In the second step, the meander pattern is defined on a 140 nm-thick HSQ mask. The pattern is then transferred to the NbN film with a (CHF_3 + SF_6 + Ar) reactive ion etching (RIE). The

#185466 - $15.00 USD Received 15 Feb 2013; revised 19 Apr 2013; accepted 22 Apr 2013; published 30 Apr 2013

patterning of the NbN nanowires (width of 100 nm, pitch of 250 nm), still covered with the HSQ mask, is very regular with a width uniformity of about 5%. In the third step we define HSQ-mask for the waveguide etching by carefully realigning this layer with the previous one. Successively, 300 nm of the underlying GaAs layer is etched with a Cl_2 + Ar electron cyclotron resonance technique. Finally, in order to allow the wiring to the TiAu electric contacts, holes through the residual HSQ-mask are opened using a PMMA mask and RIE in CHF_3 plasma. A scanning electron microscope (SEM) image of the fabricated autocorrelators is shown in Fig. 1(b).

3. Performance of waveguide autocorrelators

The experiments on waveguide autocorrelators are performed in a continuous flow cryogenic probe station with a base temperature of 2.1 K on the sample holder. A lensed fiber with a numerical aperture NA = 0.33 and corresponding spot size of 2.5 ± 0.5 μm is used to couple the light into the waveguide by the end-fire coupling method. The electrical connection to each nanowire is provided by two rf μ-probes, mounted on piezo towers. Electrical contacts are interfaced to room temperature electronics with 50Ω matched feedthrough. The signal is led through a bias tee and amplified either by 60 dB for each of the channels before being sent to the pulse counter or by 45 dB before being sent to the oscilloscope or the time-correlated single photon counting (TCSPC) module for intensity correlation measurements.

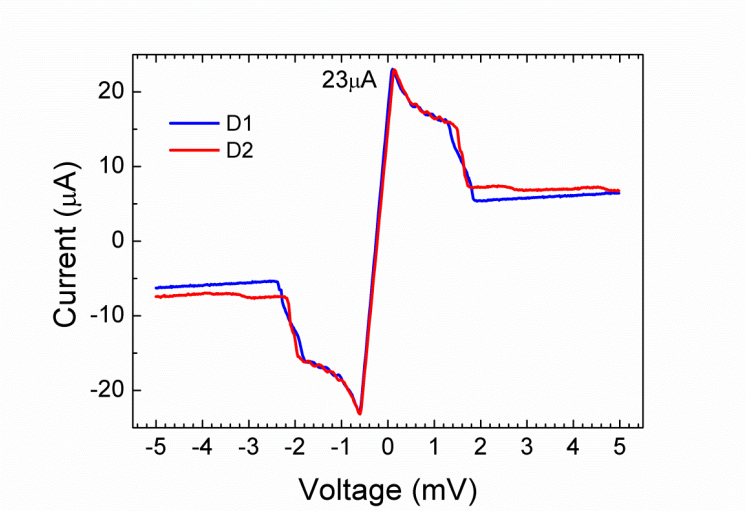

Fig. 2. Current-voltage (IV) curve of the detectors (D1, D2: see Fig. 1) on the same waveguide.

The two detectors show very similar behavior in terms of their current-voltage (IV) characteristics. As depicted in Fig. 2, both detectors have a critical current I_c = 23 μA at the measurement base temperature. Critical current density J_c is ranging between 3.4 - 3.9 MA/cm^2 for 50 μm long two-nanowire meanders.

Under illumination, photoresponse pulses with a 1/e decay time of $\tau_{1/e}$ = 1.5 ns are measured which is approximately in agreement with the calculated value $\tau_{1/e} = L_{kin}/R_{Load}$ = 1.8 ns [21], based on the kinetic inductance per square reported in Ref [22]. The difference is assigned to the different film thicknesses which is thicker for our detectors as compared to the Ref [22].

Figure 3 shows the device quantum efficiency (QE) of both detectors measured using a continuous-wave laser at 1300 nm in the TE polarization. The two detectors show very similar QE vs bias current dependences, and the peak QE value reaches to 0.5% (D1) and 0.9% (D2) at $I_b = 0.99I_c$. This value has been derived by dividing the number of counts (after subtracting the dark counts) by the number of photons coupled to the waveguide, taking into account the

#185466 - $15.00 USD Received 15 Feb 2013; revised 19 Apr 2013; accepted 22 Apr 2013; published 30 Apr 2013

measured coupling efficiency η = 16.6% and 19% for the quasi-TE and quasi-TM modes, respectively. Coupling efficiencies are determined by measuring the spectral fringes in the transmission spectra of test waveguides without NbN nanowires [6]. The dark count rate (not shown) is relatively high (~80 kHz at $I_b = 0.95I_c$) in our measurement set-up due to the non-ideal temperature and infrared background radiation but it can be reduced to <100 Hz at $I_b = 0.95I_c$ by lowering the temperature to ~1 K and better shielding of the infrared background [6]. Moreover, as shown in the inset of Fig. 3, the detectors are polarization-independent which can be attributed to the very high absorptance of the 50 μm-long wires for both polarizations. The relatively low value of the device QE, despite the high absorptance, is attributed to the limited internal QE (ratio of detected to absorbed photons) as also indicated by the unsaturated bias dependence of the QE. This is probably related to the film thickness (5.9 nm), larger than the conventional thickness used in nanowire detectors (4-5 nm).

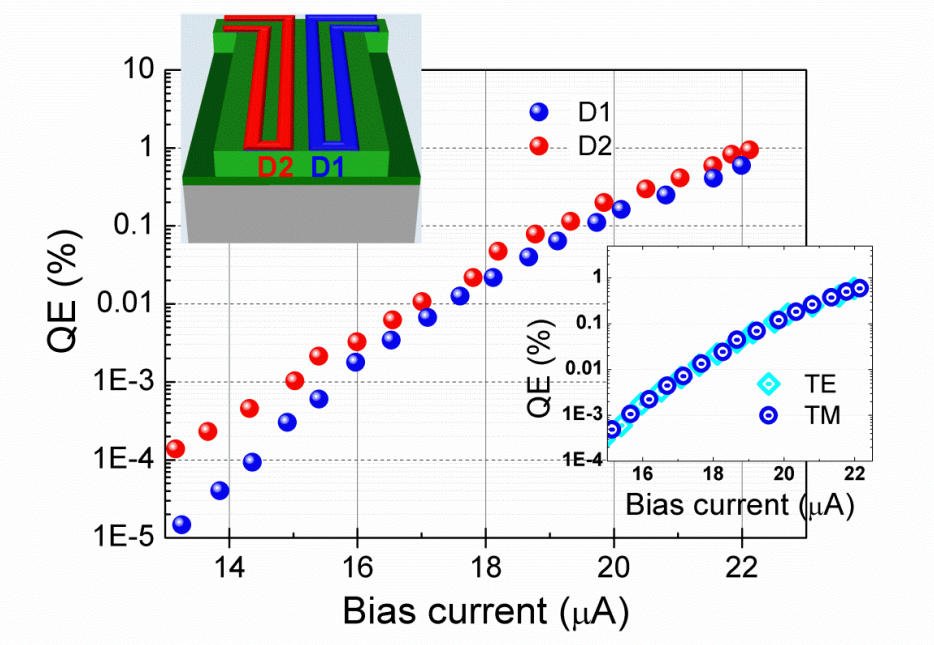

Fig. 3. Device quantum efficiency of each detector measured with TE-polarized CW light at 1300 nm (TE mode). The sketch shows the locations of the detectors. Inset: Device QE of detector D1 for TE and TM polarizations at 1300 nm.

Moreover, the quality of this NbN film is also not optimized, as indicated by the T_c, lower than previous demonstration of NbN SSPDs on GaAs [19]. We anticipate that the QE may also be increased using narrower wires [10,23].

4. Crosstalk analysis and second-order intensity correlation measurement

The close packing of the nanowires, needed to ensure equal coupling to the guided light and high absorptance, may produce electrical, magnetic or thermal coupling between the two detectors. That potentially leads to either a false detection or a decreased detection probability in one wire after the other has fired. Such coupling, which we will refer to as crosstalk in the following, would introduce spurious correlations at and around zero delays and affect the measurement of the second-order correlation function. In an ideal autocorrelator, the detectors should work independently without causing any modified/false response arising from the firing adjacent detector [14,24]. Therefore, it is of utmost importance to investigate any possible crosstalk-related limitation of our integrated autocorrelator.

#185466 - $15.00 USD Received 15 Feb 2013; revised 19 Apr 2013; accepted 22 Apr 2013; published 30 Apr 2013

Several tests are performed in order to investigate the possible crosstalk between two adjacent detectors on a single ridge waveguide. A first series of tests is performed in static conditions, to determine whether the bias condition of one detector has an influence on the electro-optical response of the other. Static coupling would mainly result from the thermal or magnetic interaction (intrinsic) as well as the coupling of two detectors due to the shared ground (extrinsic). We studied the electrical and optical response of one detector as a function of the bias of the adjacent detector. Figure 4(a) shows the IV characteristic of D1 (see Fig. 3) while D2 is unbiased. Figure 4(b) and Fig. 4(c) show the IV characteristics of D2 measured with D1 biased at the points indicated with the open squares in Fig. 4(a). In Fig. 4(b), all the curves are

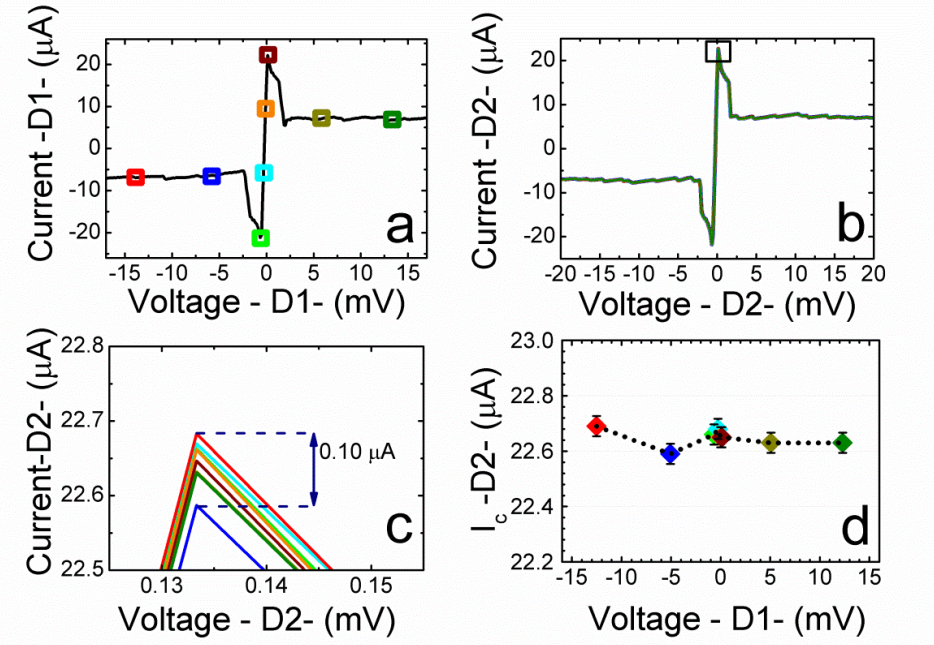

Fig. 4. (a) IV curve of the detector D1 while D2 is unbiased. (b) IV characteristic of the detector D2 at different bias conditions of D1. (c) IV curve of D2, zoomed around I_c, each curve corresponds to the bias points indicated with a square of the same color in Fig. 4(a). (d) Fluctuations in I_c of D2 while D1 is biased at several different bias conditions. The I_c is independent of the bias voltage of D1 within the error bars.

superposed while in the blow-up of Fig. 4(c) only small fluctuations (~0.10 μA) in the critical current are observed and reported in Fig. 4(d) as a function of the bias voltage of D1. It can be seen that even when the neighboring detector D1 becomes resistive, where it dissipates the Joule heating to the GaAs lattice, no change of the I_c of D2 is observed within the uncertainty (0.2%) due to stability of the experiment (see Fig. 4(d)). The same behavior is observed for the measurements by sweeping the bias voltage of D2 while measuring the IV for D1. Therefore, no static coupling between the detectors is evidenced.

This is different than the results obtained on sapphire [14] where biasing one detector in the resistive state led to a 10% decrease in the critical current of the other detector. This may be related to the higher thermal conductivity of GaAs with respect to sapphire, leading to an efficient heat transport to the substrate.

Similarly, considering the fact that the dark count rate (DCR) is very sensitive to any change, the DCR was measured for the detector D1 at several bias conditions by sweeping the bias of D2 in the superconducting and unstable region (green dots and black stars in the inset of Fig. 5 that shows the IV curve of D2 when amplifiers are connected). If switching of D2

#185466 - $15.00 USD Received 15 Feb 2013; revised 19 Apr 2013; accepted 22 Apr 2013; published 30 Apr 2013

resulted in any false counts on D1, the dark count rate of D1 would change when D2 is biased in the unstable region. Figure 5 shows the DCR of D1, biased at constant current I_b = 0.95-0.99I_c while the bias of D2 is swept. There is no measurable variation of the DCR with the bias of the other detector. That confirms that there is no measurable static coupling between two integrated WSPDs.

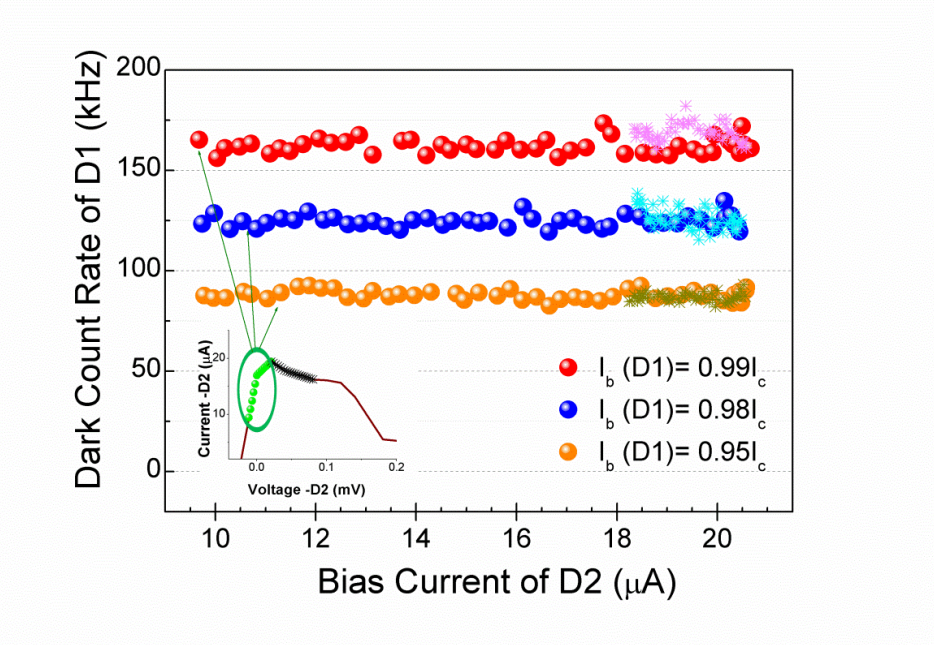

Fig. 5. The dark count rate of D1 as a function of the bias current of D2. Even when the critical current of D2 is overcome (shown by light pink, light blue and dark yellow stars folded on the original curve), the count rate of D1 does not change significantly. Inset: The IV curve of D2 where green dots show the D2 bias points in the superconducting region for which the dotted data points in the main panel are taken and the black stars show the bias points in the unstable region (colored stars in the main panel).

We then studied dynamic crosstalk, i.e. a temporal variation of the detection probability of one detector due to the firing of the other detector. To this aim, we measured the intensity correlation function $g^{(2)}(\tau)$ of both CW and pulsed laser coupled to the waveguide. As a coherent beam has a constant $g^{(2)}(\tau)$, any variation observed at small delays would indicate a spurious increase or decrease of the detection probability upon firing of the adjacent detector. The expected time range for crosstalk is within a few ns delay because the relevant timescales are the time for the formation and the decay of the hotspot (tens of ps) [25,26], the recovery time of the detector (~5 ns) [6], the electromagnetic wave travelling time between the nanowires and along the waveguide (<1 ps) as well as the propagation time of phonons across the entire detector length and between the adjacent pairs (up to a few ps).

The coincidence counts between the two detectors are measured by sending their outputs to the inputs of a correlation card (PicoHarp 300). The zero delay is calibrated in a subsequent experiment by measuring the zero-crossing of a single detector, using the same delay line. In Fig. 6, the coincidence counts are shown as a function of the delay time between the start and the stop channels for a CW light with an excitation power of 77 pW at 1300 nm at I_b = 0.97I_c (blue line) and I_b = 0.99I_c (green line). The change in the bias current modifies the number of coincidences due to the varying efficiency of the detectors (see Fig. 3). In order to improve the signal to noise ratio and to clearly observe the coincidences around zero delay, the data is averaged over a 1 ns temporal window (black lines). Even when the bias current of each

#185466 - $15.00 USD Received 15 Feb 2013; revised 19 Apr 2013; accepted 22 Apr 2013; published 30 Apr 2013

detector is brought very close to I_c, no trace of crosstalk has been observed in the vicinity of zero delay.

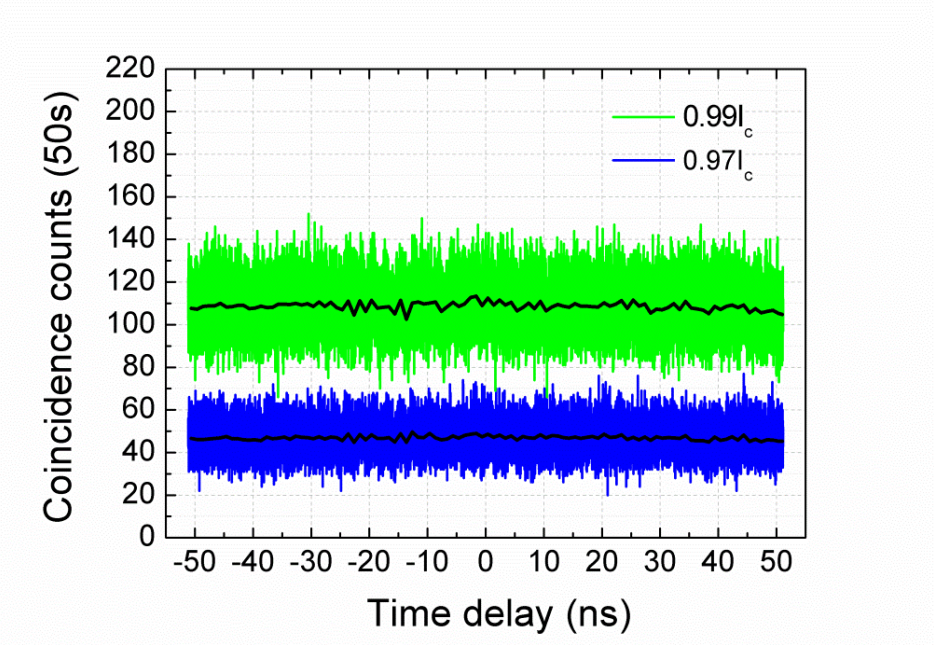

Fig. 6. Measured intensity correlation histograms for a 1300 nm CW laser with 77 pW excitation power. The detectors are biased at 99% (green line) and 97% (blue line) of their critical current. The black lines show the averaging of the data over 1 ns.

As a further test, we carried out the same experiment with a pulsed laser at 1064 nm and with 5.6 ps-long pulses and a 63 ± 0.5 MHz repetition rate. Figure 7 presents the coincidence rate as a function of time delay, measured at varying bias conditions of the two detectors. The detectors are biased with a current from $0.95I_c$ to $0.99I_c$ and data is collected for long enough to provide a high number of coincidences for the analysis and then divided by integration time to obtain the coincidence rate. In this situation, coincidences are observed only at delays multiple of the repetition period of the laser (15.9 ± 0.1 ns). The total coincidences with a 2 ns (+/– 1 ns for each side) time window around each peak are calculated and shown in Fig. 7 on the right axis and fitted with a linear curve (dashed lines). The linear fit is an approximation for the exponential decay due to the expected saturation of the coincidences vs delay, related to the relatively high count rate in this experimental condition. In order to estimate the error bar we calculate the standard deviation of the data points at delays different than zero with respect to the value given by the linear fit. For all currents, the measured coincidences at zero delay fall within the expected interval as defined by the linear fit and the error bar, showing the absence of crosstalk within our experimental accuracy of max ~4% at $0.97\text{-}0.99I_c$.

Finally, we can determine the timing resolution (jitter) from the second-order intensity correlation measurements. A total jitter of 125 ps is measured, defined as the full-width at half-maximum (FWHM) of the Gaussian distribution at zero delay, for all bias currents between $0.94I_c$ and $0.99I_c$. The jitter is the convolution of all the jitters in the measurement set-up. As the jitter of the laser and the correlation card are negligible, we only consider two detectors with an equal timing jitter (amplifiers and the cabling are not excluded) [27]. A jitter of 88 ps (FWHM) is obtained for each detector.

#185466 - $15.00 USD Received 15 Feb 2013; revised 19 Apr 2013; accepted 22 Apr 2013; published 30 Apr 2013

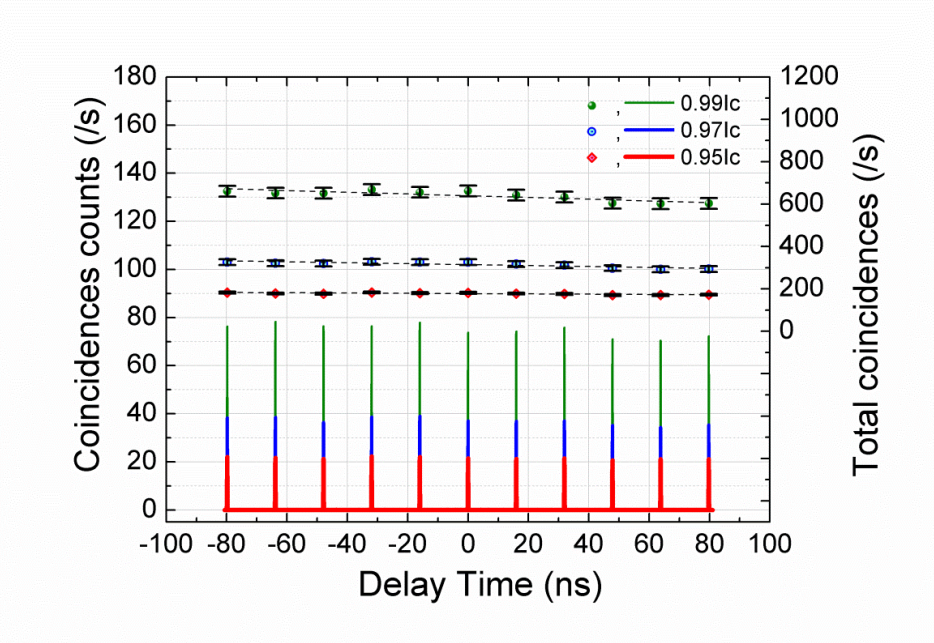

Fig. 7. Left axis: Coincidence rate under illumination with a 63 MHz pulsed laser at 1064 nm with an average power of 34 pW. The detectors are biased at 0.99 (green line), 0.97 (blue line), and 0.95 (red line) of the critical current. Right axis: Total coincidence rate at each peak points (integrated over the peak, +/– 1 ns). The black dash lines are linear fits to the data.

5. Conclusion

In conclusion, the first waveguide autocorrelators have been fabricated and measured with no crosstalk in both static and dynamic regimes within our measurement accuracy, which makes them promising candidates for on-chip autocorrelators. That allows successfully performing on-chip second-order intensity correlation measurements. As a proof of principle, the $g^{(2)}(\tau)$ of CW and pulsed light sources is measured with total temporal resolution of 125 ps (FWHM). Moreover, the detectors are shown to be polarization independent.

These waveguide autocorrelators are also the first step towards integrated photon number resolving (PNR) detectors which could be realized by connecting the different wires together in a parallel [15] or series [16] configuration. The absence of crosstalk is an essential feature for such PNR detectors whose fidelity would otherwise be affected.

Acknowledgments

This work was financially supported by the Dutch Technology Foundation STW, applied science division of NWO, the Technology Program of the Ministry of Economic Affairs, the European Commission through FP7 QUANTIP (Contract No. 244026) and Q-ESSENCE (Contact No. 248095). Part of the nanofabrication was carried out in the NanoLab@TU/e cleanroom facility.